Turkish Journal of Electrical Engineering & Computer Sciences

http://journals.tubitak.gov.tr/elektrik/

Research Article

Turk J Elec Eng & Comp Sci
(2019) 27: 649 – 662

doi:10.3906/elk-1707-319

On the stability of inverse dynamics control of flexible-joint parallel manipulators in the presence of modeling error and disturbances

Sıtkı Kemal İDER[1,*], **Ozan KORKMAZ**[2], **Mustafa Semih DENİZLİ**[1]
[1]Department of Mechanical Engineering, Faculty of Engineering, Çankaya University, Ankara, Turkey
[2]Defense Industries R&D Institute, Scientific and Technological Research Council of Turkey (TÜBİTAK SAGE), Ankara, Turkey

Received: 25.07.2017 • **Accepted/Published Online:** 03.04.2018 • **Final Version:** 22.01.2019

Abstract: Inverse dynamics control is considered for flexible-joint parallel manipulators in order to obtain a good trajectory tracking performance in the case of modeling error and disturbances. It is known that, in the absence of modeling error and disturbance, inverse dynamics control leads to linear fourth-order error dynamics, which is asymptotically stable if the feedback gains are chosen to make the real part of the eigenvalues of the system negative. However, when there are modeling errors and disturbances, a linear time-varying error dynamics is obtained whose stability is not assured only by keeping the real parts of the frozen-time eigenvalues of the system negative. In this paper, the stability of such systems is investigated and it is proved that the linear time-varying system can be rendered stable by selecting the feedback gains such that the variation of the system becomes sufficiently slow. To illustrate the performance of the control method, deployment motion of a 3-RPR planar parallel manipulator subject to impact is simulated. For the impact model, the impulse-momentum and the coefficient of restitution equations for the system are derived.

Key words: Flexible joint, stability of inverse dynamics control, parallel manipulator, impact dynamics

1. Introduction

Owing to their closed-loop structure, parallel manipulators have been widely popular for many years, especially for applications that demand precise positioning and high load-carrying capacity. Some examples of real-time applications are flight simulators, space manipulators, and robots used in medical applications.

In order to carry high loads with high motion accuracy, flexibilities in the manipulator structure should also be considered in the control system design. Joint flexibility is an important type of flexibility, which takes place due to transmission elements like couplings and harmonic drives. Good et al. [1] showed experimentally that if joint flexibility is ignored in controller design of industrial manipulators, significant performance degradation occurs.

For the motion control of parallel manipulators involving joint flexibility in their drives, the following studies can be mentioned. Liu et al. [2] designed an acceleration feedback controller to suppress the elastic vibration caused by harmonic drives. Zhao et al. [3] performed kinematic analysis of a planar flexible-joint parallel 3-RRR manipulator. Rong et al. [4] proposed a flexible spherical joint for parallel manipulators and derived its kinematic equations. Ider and Korkmaz [5] proposed an inverse dynamics control law for flexible-joint

*Correspondence: kider@cankaya.edu.tr

parallel manipulators by using feedback of velocities and positions of the rotors and actuated joints. Korkmaz and Ider [6] extended this approach to hybrid motion/force control of parallel robots working in a constrained environment.

The main objective of this study is to address the stability of inverse dynamics control of flexible-joint parallel manipulators in the presence of modeling error and disturbances for which a fourth-order, linear time-varying, nonhomogeneous error dynamics is obtained. It is known that stability is not assured by merely having the real parts of the poles negative at all times. In this paper it is analytically proved that stability can be achieved by a proper selection of the feedback gains such that the magnitude of the real part of the most dominant eigenvalue is kept in time sufficiently large. The requirements for reducing the steady-state errors are also derived.

The performance of the algorithm is demonstrated by simulations of a 3-RPR planar parallel manipulator. The case study includes impact with an object as a challenging control application, since it is a dynamic loading that causes jumps in system velocities and induces severe vibrations. In real life, collisions can take place in many applications like surgical manipulations and payload capturing operations of space robots. The adverse effects of impact on the motion accuracy are even more pronounced due to the flexibilities in the system. In order to simulate the feedback variables during impact, an impact dynamics model of the system is needed. Although there are many studies in the literature on modeling and simulation of serial robotic manipulator collisions, with or without link or joint flexibility [7–10], impact dynamics of parallel manipulators has not been addressed before. Impact dynamics of flexible-joint parallel manipulators is modeled by deriving the impulse-momentum equations of the system and the equation involving the coefficient of restitution of impact. At the impact time, the velocity jump, the impulse of the impact force, and the impulses of the loop closure constraint forces are obtained and the states of the system are updated accordingly to generate the effects of the impact on the manipulator motion.

2. Dynamic equations of flexible-joint parallel manipulator

Let an n degree of freedom parallel manipulator be transformed into an m degree of freedom open-loop structure by separating a necessary and sufficient number of unactuated joints. Then the parallel manipulator has $m-n$ independent loop closure constraint equations, which are obtained by reconnecting the separated joints. One can denote the joint variable vector of the open-loop system as:

$$\bar{\eta}=\begin{bmatrix} \bar{\eta}^{a^T} & \bar{\eta}^{u^T} \end{bmatrix}^T \tag{1}$$

where $\bar{\eta}^a$ is the $(n\times 1)$ vector of the actuated joint variables and $\bar{\eta}^u$ is the $(m-n)\times 1$ vector of the unactuated joint variables.

At an actuated joint, joint elasticity of the power transmission elements is modeled as a torsional spring [5,11]. Due to elastic transmission between the actuators and the links, additional degrees of freedom appear. At each actuator the rotor is modeled as a fictional link and so n degrees of freedom are added to the system. The ith actuator variable ϕ_i is the rotor angle of the ith actuator divided by the speed reducer ratio r_i of that actuated joint. $\bar{\phi}=[\phi_1,\ldots,\phi_n]^T$ represents the vector of the actuator variables. Actuator torques at the reducer output are denoted as T_i, $i=1,\ldots,n$ and the torsional spring constant reduced to the speed reducer output is denoted as k_i, $i=1,\ldots.n$.

The loop closure equations of the disconnected joints can be expressed in the form $g_i(\eta_1,\ldots,\eta_m)=0$,

$i=1,\cdots,m-n$. The closed-loop constraints at velocity level are:

$$\hat{B}\dot{\bar{\eta}}=\hat{B}^a\dot{\bar{\eta}}^a+\hat{B}^u\dot{\bar{\eta}}^u=\bar{0} \tag{2}$$

where $\hat{B}=\begin{bmatrix}\hat{B}^a & \hat{B}^u\end{bmatrix}$ is an $(m-n)\times m$ constraint Jacobian matrix with $B_{ij}=\frac{\partial g_i}{\partial \eta_j}$, $j=1,\ldots,m$, $i=1,\ldots,m-n$, and $\hat{B}^a$ and $\hat{B}^u$ are $(m-n)\times n$ and $(m-n)\times(m-n)$ matrices, respectively.

The gear reduction ratio is assumed to be large enough so that the rotor kinetic energy is generally due to its own rotation [5,11]. This assumption eliminates the inertia coupling between $\bar{\eta}$ and $\bar{\phi}$. Also neglecting the frictional losses in the system, the resulting equations of motion are obtained:

$$\hat{M}\ddot{\bar{\eta}}+\bar{Q}+\bar{F}^s+\hat{B}^T\bar{\lambda}=\bar{0} \tag{3}$$

$$\hat{I}^r\ddot{\bar{\phi}}-\hat{K}\left(\bar{\eta}^a-\bar{\phi}\right)=\bar{T} \tag{4}$$

Here $\hat{M}(\bar{\eta})$ is the $m\times m$ positive definite and symmetric generalized inertia matrix and $\bar{Q}(\bar{\eta},\dot{\eta})$ is the $m\times 1$ vector of gravitational, centrifugal, and Coriolis terms. $\bar{Q}$ and $\hat{M}$ are the same as those of the rigid joint open-loop system, where the rotors are considered as parts of the links on which they are mounted. $\bar{F}^s$ is an $m\times 1$ vector that contains joint spring forces such that $\bar{F}^s=\begin{bmatrix}\hat{K}\left(\bar{\eta}^a-\bar{\phi}\right)\\ \bar{0}\end{bmatrix}$, where $\hat{K}$ is an $n\times n$ diagonal stiffness matrix with $K_{ii}=k_i$ $i=1,\ldots,n$ $\hat{I}^r$ is an $n\times n$ diagonal matrix of the rotor inertias reduced to the reducer output, i.e. $I^r_{ii}=I^r_i r_i^2$, where I^r_i is the moment of inertia of the ith rotor about its rotation axis. $\bar{T}$ is the $n\times 1$ vector of the actuator torques after the speed reduction. $\hat{B}^T\bar{\lambda}$ is the vector of generalized loop closure constraint forces where $\bar{\lambda}$ represents the $(m-n)\times 1$ vector of the joint reaction forces at the disconnected joints.

One can reduce the manipulator equations of motion by eliminating the unactuated joint accelerations $\ddot{\bar{\eta}}^u$ and the constraint forces $\bar{\lambda}$ in Eq. (3). To this end, $\ddot{\bar{\eta}}^u$ is obtained by differentiating Eq. (2) as:

$$\ddot{\bar{\eta}}^u=-\left(\hat{B}^u\right)^{-1}\left[\hat{B}^a\ddot{\bar{\eta}}^a+\dot{\hat{B}}^a\dot{\bar{\eta}}^a+\dot{\hat{B}}^u\dot{\bar{\eta}}^u\right]. \tag{5}$$

Using adequate partitioning of $\hat{M}$ and $\bar{Q}$ according to $\bar{\eta}^a$ and $\bar{\eta}^u$ as $\hat{M}=\begin{bmatrix}\hat{M}^{aa} & \hat{M}^{au}\\ \hat{M}^{auT} & \hat{M}^{uu}\end{bmatrix}$ and $\bar{Q}=\begin{bmatrix}\bar{Q}^a\\ \bar{Q}^u\end{bmatrix}$ in Eq. (3), substituting Eq. (5), and eliminating $\bar{\lambda}$ yields the following n-dimensional equation for the closed-loop system [5]:

$$\hat{M}^\star\ddot{\bar{\eta}}^a+\bar{Q}^\star+\hat{K}\left(\bar{\eta}^a-\bar{\phi}\right)=\bar{0}, \tag{6}$$

where:

$$\hat{M}^\star=-\hat{B}^{a^T}\left(\hat{B}^{u^{-1}}\right)^T\left[\hat{M}^{au^T}-\hat{M}^{uu}\hat{B}^{u^{-1}}\hat{B}^a\right]+\left[\hat{M}^{aa}-\hat{M}^{au}\hat{B}^{u^{-1}}\hat{B}^a\right] \tag{7}$$

$$\begin{aligned}\bar{Q}^\star=&\left[-\hat{M}^{au}\hat{B}^{u^{-1}}\dot{\hat{B}}^a+\hat{B}^{a^T}\left(\hat{B}^{u^{-1}}\right)^T\hat{M}^{uu}\hat{B}^{u^{-1}}\dot{\hat{B}}^a\right]\dot{\bar{\eta}}^a\\&+\left[-\hat{M}^{au}\hat{B}^{u^{-1}}\dot{\hat{B}}^u+\hat{B}^{a^T}\left(\hat{B}^{u^{-1}}\right)^T\hat{M}^{uu}\hat{B}^{u^{-1}}\dot{\hat{B}}^u\right]\dot{\bar{\eta}}^u+\bar{Q}^a-\hat{B}^{a^T}\left(\hat{B}^{u^{-1}}\right)^T\bar{Q}^u.\end{aligned} \tag{8}$$

3. Inverse dynamics control of flexible-joint parallel manipulator

The inverse dynamics control technique basically depends on finding the input/output relation. The inputs of the system are the actuator torques/forces and the outputs are the end-effector position variables.

Let x_i, $i = 1, \ldots, n$ stand for the Cartesian position variables of the end effector. The task equations that relate the coordinates of the end effector with the joint coordinates can be expressed in the form $x_i = f_i(\eta_1, \ldots, \eta_m)$, $i = 1, \ldots, n$. At velocity level, the task equations can be expressed as:

$$\dot{\bar{x}} = \hat{\Gamma}\dot{\bar{\eta}} = \begin{bmatrix} \hat{\Gamma}^a & \hat{\Gamma}^u \end{bmatrix} \begin{Bmatrix} \dot{\bar{\eta}}^a \\ \dot{\bar{\eta}}^u \end{Bmatrix} = \hat{\Gamma}^a \dot{\bar{\eta}}^a + \hat{\Gamma}^u \dot{\bar{\eta}}^u, \tag{9}$$

where $\hat{\Gamma}^a$ is an $n \times n$ matrix and $\hat{\Gamma}^u$ is an $n \times (m-n)$ matrix with $\Gamma^a_{ij} = \frac{\partial f_i}{\partial \eta^a_j}$ and $\Gamma^u_{ij} = \frac{\partial f_i}{\partial \eta^u_j}$.

By making use of Eq. (2), one can eliminate $\dot{\bar{\eta}}^u$ in Eq. (9), yielding:

$$\dot{\bar{x}} = \hat{J}\dot{\bar{\eta}}^a \tag{10}$$

where $\hat{J} = \hat{\Gamma}^a - \hat{\Gamma}^u \hat{B}^{u^{-1}} \hat{B}^a$ is an $n \times n$ robot Jacobian matrix.

In order to find the relation between the output $\bar{x}$ and input torques $\bar{T}$, one can substitute $\hat{K}\left(\bar{\eta}^a - \bar{\phi}\right)$ obtained from Eq. (6) and $\ddot{\bar{\phi}}$ obtained from the second derivative of Eq. (6) into Eq. (4), and then substitute $\dddot{\bar{\eta}}^a$ obtained from the third derivative of Eq. (10) into the resulting equation:

$$\hat{A}\dddot{\bar{x}} + \bar{B} = \bar{T} + \bar{D}. \tag{11}$$

Here,

$$\hat{A} = \hat{K}^{-1}\hat{I}^r\hat{M}^*\hat{J}^{-1} \tag{12}$$

$$\begin{aligned} \bar{B} = &- \hat{K}^{-1}\hat{I}^r\hat{M}^*\hat{J}^{-1}\left(3\dot{\hat{J}}\ddot{\bar{\eta}}^a + 3\ddot{\hat{J}}\dot{\bar{\eta}}^a + \dddot{\hat{J}}\bar{\eta}^a\right) + 2\hat{K}^{-1}\hat{I}^r\dot{\hat{M}}^* \\ &+ \hat{K}^{-1}\hat{I}^r\ddot{\hat{M}}^*\dot{\bar{\eta}}^a + \hat{K}^{-1}\hat{I}^r\hat{K}\ddot{\bar{\eta}}^a + \hat{K}^{-1}\hat{I}^r\ddot{\bar{Q}}^* + \hat{M}^*\ddot{\bar{\eta}}^a + \bar{Q}^*, \end{aligned} \tag{13}$$

and $\bar{D}$ stands for the generalized disturbance force vector.

When $\hat{J}$ is singular the parallel manipulator is at a kinematic singularity at which the manipulator loses at least one degree of freedom, and when $\hat{B}^u$ is singular it is at a drive singularity at which control of the manipulator is lost by the actuators in some directions [12]. In this study it is assumed that the chosen trajectory avoids such singular positions so that $\hat{J}$ and $\hat{B}^u$ are always nonsingular.

Using Eq. (11), an inverse dynamics control law can be formulated by selecting the control torques as follows:

$$\bar{T} = \hat{A}_{est}\bar{u} + \bar{B}_{est}, \tag{14}$$

where $\bar{u}$ is an $n \times 1$ control vector, which represents command snaps:

$$\bar{u} = \dddot{\bar{x}}^d + \hat{C}_1\left(\ddot{\bar{x}}^d - \ddot{\bar{x}}\right) + \hat{C}_2\left(\dot{\bar{x}}^d - \dot{\bar{x}}\right) + \hat{C}_3\left(\bar{x}^d - \bar{x}\right) + \hat{C}_4\left(\bar{x}^d - \bar{x}\right), \tag{15}$$

where the superscript d indicates desired values and $\hat{C}_i$, $i=1,\ldots,4$ are constant $n\times n$ feedback gain diagonal matrices with diagonal elements C_{ij}, $j=1,\ldots,n$. The subscript est in Eq. (14) specifies the estimated values, which are different than the actual values due to modeling error. Due to the linearizing effect of the control law expressed by Eq. (14), Eq. (11) is reduced to:

$$\dddot{\bar{x}}=\hat{E}\bar{u}-\hat{A}^{-1}\left(\bar{B}-\bar{B}_{est}\right)+\hat{A}^{-1}\bar{D}, \tag{16}$$

where:

$$\hat{E}=\hat{A}^{-1}\bar{A}_{est}. \tag{17}$$

Substitution of Eq. (15) into Eq. (16) yields the following error dynamics:

$$\dddot{\bar{e}}+\hat{E}\hat{C}_1\ddot{\bar{e}}+\hat{E}\hat{C}_2\dot{\bar{e}}+\hat{E}\hat{C}_3\dot{\bar{e}}+\hat{E}\hat{C}_4\bar{e}=\bar{\delta}\,, \tag{18}$$

where $\bar{e}=\bar{x}^d-\bar{x}$ and the effective disturbance $\bar{\delta}$ is obtained as

$$\bar{\delta}=\hat{A}^{-1}\left(\bar{B}-\bar{B}_{est}\right)+\left(\hat{I}-\hat{E}\right)\dddot{\bar{x}}^d-\hat{A}^{-1}\bar{D}. \tag{19}$$

The measurements required by the control law are the velocities and positions of the actuator rotors and the actuated joints, i.e. $\dot{\bar{\eta}}^a$, $\bar{\eta}^a$, $\dot{\bar{\phi}}$ and $\bar{\phi}$. The other unknown variables in the control law are obtained using these measured variables. In particular, $\ddot{\bar{\eta}}^a$ and $\dddot{\bar{\eta}}^a$ are found using Eq. (6) and its derivative where the parameters may involve modeling error, i.e.

$$\ddot{\bar{\eta}}^a=-\hat{M}^{*-1}_{est}\left[\bar{Q}^*_{est}+\hat{K}_{est}\left(\bar{\eta}^a-\bar{\phi}\right)\right], \tag{20}$$

$$\dddot{\bar{\eta}}^a=-\hat{M}^{*-1}_{est}\left[\dot{\hat{M}}^*_{est}\ddot{\bar{\eta}}a+\dot{\bar{Q}}^*_{est}+\hat{K}_{est}\left(\dot{\bar{\eta}}^a-\dot{\bar{\phi}}\right)\right] \tag{21}$$

During the control simulations the measured variables for each sampling time are obtained by forward dynamics simulation. To this end, substituting the control torques obtained from Eq. (14), $\ddot{\bar{\eta}}^a$ and $\ddot{\bar{\phi}}$ are calculated by making use of Eqs. (6) and (4). Then $\dot{\bar{\eta}}^a$, $\bar{\eta}^a$, $\dot{\bar{\phi}}$, and $\bar{\phi}$ are obtained by numerical integration.

4. Stability of the control system

Since $\hat{A}$ is positive definite, using an appropriate positive definite estimate of $\hat{A}$, the matrix $\hat{E}$ defined by Eq. (17) comes out to be a positive definite matrix, too. On the other hand, $\hat{E}\cong\hat{I}$ provided that $\hat{A}_{est}\cong\hat{A}$.

Eq. (18) represents a linear time-varying system. In the case that there is no modeling error ($\hat{E}\cong\hat{I}$ and $\bar{B}=\bar{B}_{est}$), Eq. (18) reduces to the following equation that describes the linear time-invariant version of the same system:

$$\dddot{\bar{e}}+\hat{C}_1\ddot{\bar{e}}+\hat{C}_2\dot{\bar{e}}+\hat{C}_3\dot{\bar{e}}+\hat{C}_4\bar{e}=0\ . \tag{22}$$

Asymptotic stability of the system described by Eq. (22) can be achieved by suitable selection of the feedback gain diagonal matrices. ITAE, IAE, critically damped, etc. criteria can be used for this purpose. Without losing generality, let the ITAE criterion be used. In this case the diagonal elements of the feedback gain matrices are $C_{1j}=2.1\,\omega_j$, $C_{2j}=3.4\,\omega_j^2$, $C_{3j}=2.7\,\omega_j^3$, $C_{4j}=\omega_j^4$ for all $j=1,\ldots,n$, where ω_j are positive constants.

Since $\hat{E} \cong \hat{I}$ one can choose ω_j large enough such that the real parts of all poles of the system described by Eq. (18) are still negative. To investigate the stability of the actual linear time-varying system described by Eq. (18), consider the following state representation based on Eq. (18):

$$\dot{\bar{\mu}} = \hat{\Upsilon}(t)\,\bar{\mu}, \tag{23}$$

where:

$$\bar{\mu}^T = \begin{bmatrix} \bar{e}^T & \bar{p}^T & \bar{q}^T & \bar{r}^T \end{bmatrix}, \tag{24}$$

$$\hat{\Upsilon}(t) = \begin{bmatrix} \hat{0} & \hat{I} & \hat{0} & \hat{0} \\ \hat{0} & \hat{0} & \hat{I} & \hat{0} \\ \hat{0} & \hat{0} & \hat{0} & \hat{I} \\ -\hat{E}\hat{C}_4 & -\hat{E}\hat{C}_3 & -\hat{E}\hat{C}_2 & -\hat{E}\hat{C}_1 \end{bmatrix}, \tag{25}$$

$\bar{p} = \dot{\bar{e}}, \bar{q} = \dot{\bar{p}}$, and $\bar{r} = \dot{\bar{q}}$. It is known that asymptotic stability is not assured by only having a stability margin $\sigma_o > 0$ such that

$$Re\lambda_i(t) \leq -\sigma_o \forall i,\ \forall t \geq 0, \tag{26}$$

where λ_i is the ith eigenvalue (pole) of $\hat{\Upsilon}(t)$ [13,14]. However, it is known that such a system is asymptotically stable if the variation of $\hat{\Upsilon}(t)$ is sufficiently slow. Desoer [13] showed that Eq. (23) is asymptotically stable at large if

$$\Delta_M \leq \frac{\sigma_o^2}{3m^4}, \tag{27}$$

where

$$\Delta_M = sup_{t\geq 0} \left\| \dot{\hat{\Upsilon}}(t) \right\| \tag{28}$$

and m is a constant that satisfies

$$\left\| e^{\hat{\Upsilon}(t)} \right\| \leq m\, e^{-\tau\left(\frac{\sigma_o}{2}\right)} \forall t \geq 0, \forall \tau \geq 0. \tag{29}$$

To see how σ_o affects Eq. (27), consider how Δ_M varies with σ_o. $\dot{\hat{\Upsilon}}(t)$ can be expressed as:

$$\dot{\hat{\Upsilon}}(t) = \begin{bmatrix} \hat{0} & \hat{0} & \hat{0} & \hat{0} \\ \hat{0} & \hat{0} & \hat{0} & \hat{0} \\ \hat{0} & \hat{0} & \hat{0} & \hat{0} \\ -\dot{\hat{E}}\hat{C}_4 & -\dot{\hat{E}}\hat{C}_3 & -\dot{\hat{E}}\hat{C}_2 & -\dot{\hat{E}}\hat{C}_1 \end{bmatrix}. \tag{30}$$

Since $\dot{\hat{E}}(t)$ is independent of λ_i, $i = 1, \cdots, n$, the effect of λ_i on $\dot{\hat{\Upsilon}}(t)$ is in the order of λ_i. This is because the poles of $\hat{\Gamma}(t)$ are placed directly by means of $\hat{C}_i$, $i = 1, \ldots, 4$. On the other hand, $\sigma_o = min_{t\geq 0}[Re\,\lambda_1]$, where λ_1 is the most dominant eigenvalue. Therefore, the effect of σ_o on Δ_M is in the order of σ_o, while the effect of σ_o on the RHS of Eq. (27) is in the order of σ_o^2. Hence, by choosing a sufficiently large σ_o, the variation of $\hat{\Upsilon}(t)$ becomes slow compared to the dynamics of the system and one achieves asymptotic stability in the large.

Therefore, with larger values of ω_j for all j, $|\bar{e}|$ can be decreased. This is due to the fact that the effective disturbance $\bar{\delta}$ is not a function of the natural frequencies of the system described by Eq. (18), and hence one can choose ω_j, $j=1,\ldots,n$ such that $\bar{\delta}$ appears to be changing much more slowly with regard to a signal such as $\sin(\Omega_k t)$, where Ω_k is the smallest natural frequency of the same system. Hence, after the transient phase, the error converges to the value given below in Eq. (31), which becomes smaller as the elements of $\hat{C}_4$ increase:

$$\bar{e}^*=\hat{C}_4^{-1}\hat{E}^{-1}\bar{\delta}. \tag{31}$$

5. Impact dynamics

Let a particle P of mass m_P collide with the manipulator while it is in motion at point Q, which is on the surface of the end-effector or another link. The impact is assumed to take place in a very short-lived interval of time $\tau_1\leq t\leq\tau_2$, where τ_1, and τ_2 are close enough that the system configuration does not undergo a considerable change during the impact.

The generalized impact force vector $\bar{F}^P$ due to the impact force $F^I(t)$ generated at contact point Q can be expressed as:

$$\bar{F}^P=\frac{\partial\bar{v}_Q}{\partial\dot{\bar{\eta}}}\cdot F^I\bar{z}=\hat{L}^{Q^T}\bar{z}F^I, \tag{32}$$

where $\bar{v}_Q$ is the velocity vector and $\hat{L}^Q=\frac{\partial\bar{v}_Q}{\partial\dot{\bar{\eta}}}$ is the velocity influence coefficient matrix of point Q, and $\bar{z}$ is the unit vector in the direction of the impact force. Including the generalized impact force represented by Eq. (32) to the manipulator dynamic equations, Eq. (3) takes the following form:

$$\hat{M}\ddot{\bar{\eta}}+\bar{Q}+\bar{F}^s+\hat{B}^T\bar{\lambda}+\hat{L}^{Q^T}\bar{z}F^I=\bar{0}. \tag{33}$$

Similarly, the equation of motion of the colliding particle P during impact can be expressed as below:

$$m_P\ddot{\bar{r}}_P-\hat{L}^{P^T}\bar{z}F^I=\bar{0}, \tag{34}$$

where $\hat{L}^P=\frac{\partial\bar{v}_P}{\partial\dot{\bar{r}}_P}$ is the velocity influence coefficient matrix of particle P. Since $\bar{v}_P=\dot{\bar{r}}_P$, $\hat{L}^P$ equals the 2×2 identity matrix $\hat{I}$.

In order to obtain impulse-momentum equations, the dynamic equations of the manipulator ((Eq. 33) and (4)) and the dynamic equation of the particle (Eq. (34)) are integrated over the time interval $\tau_1\leq t\leq\tau_2$ as

$$\int_{\tau_1}^{\tau_2}\left(\hat{M}\ddot{\bar{\eta}}+\bar{Q}+\bar{F}^s-\hat{B}^T\bar{\lambda}+\hat{L}^{Q^T}\bar{z}F^I\right)dt=\bar{0}, \tag{35}$$

$$\int_{\tau_1}^{\tau_2}\left[\hat{I}^r\ddot{\bar{\phi}}-\hat{K}\left(\bar{\eta}^a-\bar{\phi}\right)\right]dt=\int_{\tau_1}^{\tau_2}\bar{T}dt, \tag{36}$$

$$\int_{\tau_1}^{\tau_2}\left(m_P\ddot{\bar{r}}_P-\bar{z}F^I\right)dt=\bar{0}. \tag{37}$$

Assuming that the applied forces are continuous and noting that the positions do not change considerably and velocities are bounded during the impact period, the terms $\int_{\tau_1}^{\tau_2}\bar{T}dt$, $\int_{\tau_1}^{\tau_2}\left(\bar{Q}+\bar{F}^s\right)dt$, and $\int_{\tau_1}^{\tau_2}\left[-\hat{K}\left(\bar{\eta}^a-\bar{\phi}\right)\right]dt$

become negligible. Since $\hat{M}$, $\hat{B}$, $\hat{L}^Q$, and $\bar{z}$ depend on positions only, they almost remain constant during impact. Then Eqs. (35)–(37) reduce to:

$$\hat{M}\Delta\dot{\bar{\eta}}+\hat{B}^T\bar{\Lambda}+\hat{L}^{Q^T}\bar{z}H=\bar{0}, \tag{38}$$

$$\hat{I}^r\Delta\dot{\bar{\phi}}=\bar{0}, \tag{39}$$

$$m_P\Delta\dot{\bar{r}}_P-\bar{z}H=\bar{0}, \tag{40}$$

where $\Delta\dot{\bar{\eta}}$, $\Delta\dot{\bar{\phi}}$, and $\Delta\dot{\bar{r}}_P$ represent the jumps in the corresponding velocity vectors due to impact. H is the impulse of the impact force and $\bar{\Lambda}$ is the vector of the impulses of the loop closure constraint reaction forces, which are given as:

$$H=\int_{\tau_1}^{\tau_2}F^I dt, \tag{41}$$

$$\bar{\Lambda}=\int_{\tau_1}^{tau_2}\bar{\lambda}dt \tag{42}$$

Eq. (39) implies that $\Delta\dot{\bar{\phi}}=\bar{0}$, i.e. the vector of the rotor velocities, $\dot{\bar{\phi}}$, does not change during the impact.

The conditions that the constraint equations impose on the velocity jump during impact should also be considered. Using Eq. (2) at τ_1 and τ_2, one obtains:

$$\hat{B}\dot{\bar{\eta}}\left(\tau_2\right)-\hat{B}\dot{\bar{\eta}}\left(\tau_1\right)=\hat{B}\Delta\dot{\bar{\eta}}=\bar{0}. \tag{43}$$

It is known that the coefficient of restitution e can be expressed as:

$$e=-\bar{z}\cdot\left[\bar{v}_Q\left(\tau_2\right)-\bar{v}_P\left(\tau_2\right)\right]/\left\{\bar{z}\cdot\left[\bar{v}_Q\left(\tau_1\right)-\bar{v}_P\left(\tau_1\right)\right]\right\}. \tag{44}$$

Using $\bar{v}_Q=\hat{L}^Q\dot{\bar{\eta}}$ and $\bar{v}_P=\dot{\bar{r}}_P$, Eq. (44) takes the following form:

$$\bar{z}^T\left(\hat{L}^Q\Delta\dot{\bar{\eta}}-\Delta\dot{\bar{r}}_P\right)=-(e+1)\bar{z}^T\left[\hat{L}^Q\dot{\bar{\eta}}\left(\tau_1\right)-\dot{\bar{r}}_P\left(\tau_1\right)\right]. \tag{45}$$

Eqs. (38), (40), (43), and (45) represent $m+2+(m-n)+1=2m-n+3$ linear equations for obtaining the jump discontinuity in the velocities $\dot{\bar{\eta}}$ and $\dot{\bar{r}}_P$, the impulse vector $\bar{\Lambda}$ of the loop closure reaction forces, and the impactive impulse H. In augmented matrix form these equations are expressed as:

$$\begin{bmatrix} \hat{M} & \hat{0} & -\hat{B}^T & \hat{L}^{Q^T}\bar{z} \\ \hat{0} & m_P\hat{I} & \hat{0} & -\bar{z} \\ \hat{B} & \hat{0} & \hat{0} & \bar{0} \\ \bar{z}^T\hat{L}^Q & -\bar{z}^T & \bar{0} & 0 \end{bmatrix} \begin{Bmatrix} \Delta\dot{\bar{\eta}} \\ \Delta\dot{\bar{r}}_P \\ \bar{\Lambda} \\ H \end{Bmatrix} = \begin{Bmatrix} \bar{0} \\ \bar{0} \\ \bar{0} \\ -(e+1)\bar{z}^T\left[\hat{L}^Q\dot{\bar{\eta}}\left(\tau_1\right)-\dot{\bar{r}}_P\left(\tau_1\right)\right] \end{Bmatrix}, \tag{46}$$

where $\hat{M}$, $\hat{B}$, $\hat{L}^Q$, and $\bar{z}$ are also evaluated at $t=\tau_1$.

The impact model presented in this article is also applicable to object capturing applications. Object capturing represents a special case of general impact where the relative velocity of the contacting points after

impact is zero, i.e. impact is fully plastic, and hence the coefficient of restitution e in the above equations becomes zero.

At impact time, the velocity jump $\Delta\dot{\bar{\eta}}$ due to impact is calculated using Eq. (46). The updated velocity vector $\dot{\bar{\eta}}(\tau_2)$ is obtained by adding $\Delta\dot{\bar{\eta}}$ to the velocity vector $\dot{\bar{\eta}}(\tau_1)$, which is obtained by the forward dynamics solution. Then $\dot{\bar{\eta}}(\tau_2)$ is used as the new velocity vector for the next step, while $\dot{\bar{\phi}}$ and the position vectors remain the same.

6. Numerical example

The 3-RPR planar parallel manipulator shown in Figure 1 is considered as a case study. The robot has three legs, each containing two revolute joints and one prismatic joint between the moving platform and the fixed base. Excluding the extra degrees of freedom of the flexible-joint drives, the manipulator has 3 DOF, i.e. $n=3$. The base joints whose joint variables are θ_1, θ_3, and θ_5 are all actuated. Since the open-loop system obtained by disconnecting the joints at E and F has 7 DOF, i.e. $m=7$, the joint variable vector takes the following form:

$$\bar{\eta}=[\theta_1 \;\; \theta_3 \;\; \theta_5 \;\; \theta_7 \;\; \xi_2 \;\; \xi_4 \;\; \xi_6]^T . \tag{47}$$

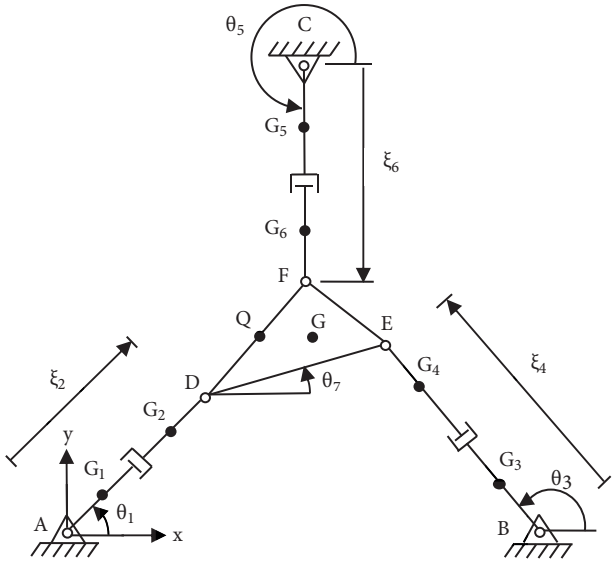

Figure 1. 3-RPR planar parallel manipulator.

Then the relevant actuated and unactuated joint variable vectors are expressed as:

$$\bar{\eta}^a=[\theta_1 \;\; \theta_3 \;\; \theta_5]^T , \; \bar{\eta}^u=[\theta_7 \;\; \xi_2 \;\; \xi_4 \;\; \xi_6]^T \tag{48}$$

The vectors of the rotor variables at the actuated joints are:

$$\bar{\phi}=[\phi_1 \;\; \phi_2 \;\; \phi_3]^T . \tag{49}$$

The fixed link dimensions are labeled as $AB=AC=CB=L$, $DE=L_7$, $DF=L_7'$, $\angle FDE=\alpha$, $\angle GDE=\beta$, $DG=g_7$, $AG_1=a_1$, $DG_2=a_2$, $BG_3=a_3$, $EG_4=a_4$, $CG_5=a_5$, $FG_6=a_6$. G_i denotes mass center of link i. G is mass center of link 7.

There are four constraint equations given by:

$$\begin{bmatrix} g_1 = \xi_2 \cos\theta_1 + L_7 cos\theta_7 - L - \xi_4 \cos\theta_3 \\ g_2 = \xi_2 \sin\theta_1 + L_7 \sin\theta_7 - \xi_4 \sin\theta_3 \\ g_3 = \xi_2 \cos\theta_1 + L_7^{'} \cos(\theta_7 + \alpha) - 0.5L - \xi_6 \cos\theta_5 \\ g_4 = \xi_2 \sin\theta_1 + L_7^{'} \sin(\theta_7 + \alpha) - 0.866L - \xi_6 \sin\theta_5 \end{bmatrix} = \begin{bmatrix} 0 \\ 0 \\ 0 \\ 0 \end{bmatrix}. \tag{50}$$

The coordinates x_G and y_G of point G and the orientation variable θ_7 of the moving platform constitute the end-effector position vector $\bar{x}$:

$$\bar{x} = \begin{bmatrix} x_G \\ y_G \\ \theta_7 \end{bmatrix} = \begin{bmatrix} \xi_2 \cos\theta_1 + g_7 \cos(\theta_7 + \beta) \\ \xi_2 \sin\theta_1 + g_7 \sin(\theta_7 + \beta) \\ \theta_7 \end{bmatrix}. \tag{51}$$

The link dimensions are $L = 2$ m, $L_7 = L_7^{'} = 0.4$ m, $a_i = 0.3$ m, $i = 1, \cdots, 6$, $g_7 = 0.231$ m, $\alpha = 60^{\circ}$ $\beta = 30^{\circ}$ The masses of the links are $m_i^L = 5$ kg, $i = 1, \cdots, 6$, $m_7^L = 7$ kg. The moments of inertia of the links about axes through mass centers are $I_{z_i} = 0.15$ kg m^2, $i = 1, \cdots, 6$, $I_{z_7} = 0.23$ kg m^2. The rotor moments of inertia about axes are $I_i^r = 2 \times 10^{-5}$ kg m^2, $i = 1, 2, 3$. The gear ratios are $r_i = 100$, $i = 1, 2, 3$. Torsional joint spring constants are $k_i = 2500$ Nm/rad, $i = 1, 2, 3$.

Initially the system is at rest, with $\theta_{1_0} = 45^{\circ}$, $\theta_{3_0} = 155^{\circ}$, and $\theta_{5_0} = 255^{\circ}$. The corresponding initial unactuated joint variables are $\theta_{7_0} = -5.38^{\circ}$, $\xi_{2_0} = 0.756$ m, $\xi_{4_0} = 1.177$ m, and $\xi_{6_0} = 0.901$ m. Initial values of the joint variables result in the following initial position vector of the end-effector:

$$\bar{x}_o = \begin{bmatrix} x_{G_o} \\ y_{G_o} \\ \theta_{7_0} \end{bmatrix} = \begin{bmatrix} 0.745\,\text{m} \\ 0.631\,\text{m} \\ -5.38^0 \end{bmatrix}. \tag{52}$$

The ITAE criterion is considered for the determination of the feedback gains. The diagonal elements of the feedback gains are $C_{1i} = 2.1\omega_i$, $C_{2i} = 3.4\omega_i^2$, $C_{3i} = 2.7\omega_i^3$, $C_{4i} = \omega_i^4$, $i = 1, 2, 3$, where ω_i are positive constants.

The following desired end-effector cycloidal deployment motion is considered:

$$x_G^d = \left\{ \begin{array}{l} 0.70 + \frac{0.35}{T}\left[t - \frac{T}{2\pi}\sin\frac{2\pi t}{T}\right] \text{m } 0 \le t < T \\ 1.05 \text{ m } t \ge T \end{array} \right\},$$

$$y_G^d = \left\{ \begin{array}{l} 0.60 + \frac{0.20}{T}\left[t - \frac{T}{2\pi}\sin\frac{2\pi t}{T}\right] \text{m } 0 \le t < T \\ 0.80 \text{ m } t \ge T \end{array} \right\}, \tag{53}$$

$$\theta_7^d = \left\{ \begin{array}{l} 0 + \frac{25}{T}\left[t - \frac{T}{2\pi}\sin\frac{2\pi t}{T}\right] \text{deg.} 0 \le t < T \\ 25 \text{ deg. } t \ge T \end{array} \right\},$$

where $T = 1.0$ s, which is the period of deployment motion. Considering Eqs. (52) and (53), there exist initial position errors in all components of the end-effector position vector. Also, the desired jerks have discontinuities at the boundaries. In the simulations, modeling error is taken into account such that the robot mass and inertia

parameters and the stiffness constants are taken to be 10% smaller in the model. The sampling time interval is taken as h= 0.002 s (sampling frequency is 3142 rad/s).

The impact scenario is set up in such a way that, at time t = 0.25 s, a particle having mass m_P= 5 kg hits point Q of link 7 with velocity $\dot{\bar{r}}_P$= $\left[\begin{array}{cc} 1.5 & -1 \end{array}\right]^T$ m/s, where DQ =b_7= 0.15 m. The coefficient of restitution is assumed to be e= 0.9. The velocity influence coefficient matrix $\hat{L}^Q$ of point Q takes the following form:

$$\hat{L}^Q = \left[\begin{array}{cccccccc} -\xi_2 \sin\theta_1 & 0 & 0 & -b_7 \sin(\theta_7+\alpha) & \cos\theta_1 & 0 & 0 \\ \xi_2 \cos\theta_1 & 0 & 0 & b_7 \cos(\theta_7+\alpha) & \sin\theta_1 & 0 & 0 \end{array}\right]. \tag{54}$$

The unit vector $\bar{z}$ along the normal direction is obtained as:

$$\bar{z} = \left\{\begin{array}{c} \cos(\theta_7+\alpha+270^o) \\ \sin(\theta_7+\alpha+270^o) \end{array}\right\}. \tag{55}$$

The closed-loop position and velocity responses, elastic deflections, and actuator torques $T_i^* = T_i/r_i$, i= 1, 2, 3 are displayed in Figures 2, 3, and 4, for ω_i= 50 rad/s. The magnitudes of the velocity jumps due to impact are visible in Figure 3. Figure 4 reveals the corresponding jumps in the actuator torques. It is assumed that actuators provide sufficient torques so that there is no saturation. Despite the effects of initial position errors, modeling error, and velocity jumps due to impact, satisfactory tracking performance is achieved at all end-effector position variables.

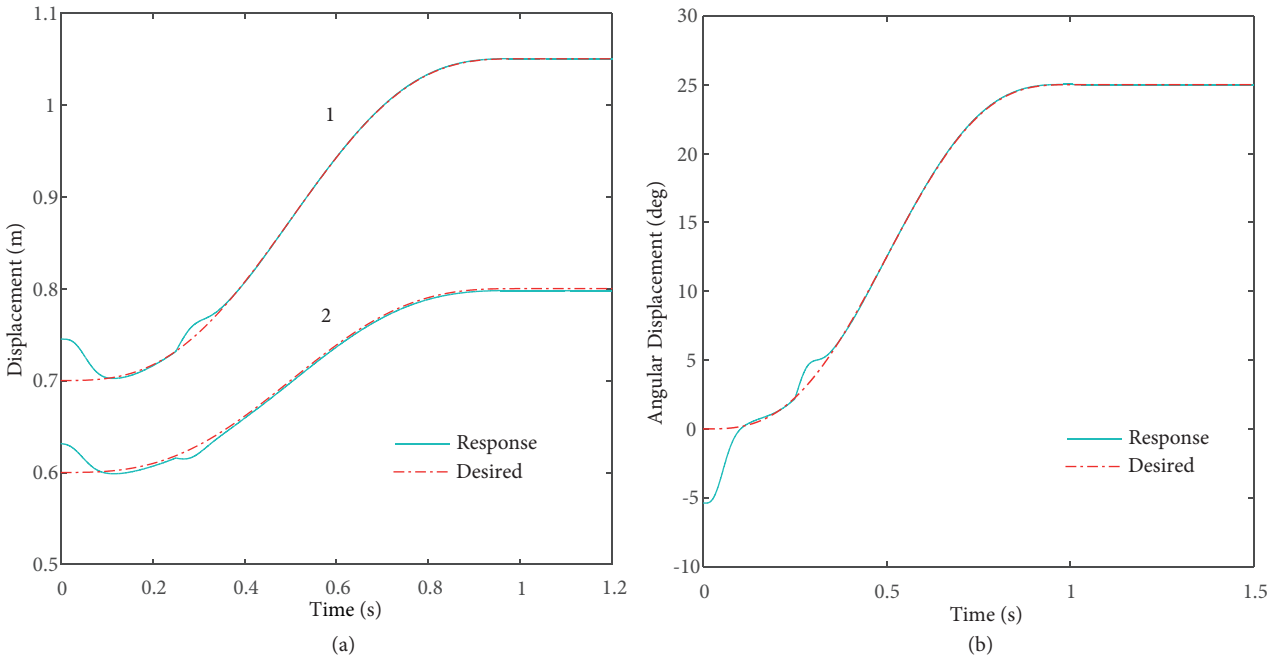

Figure 2. Position responses: (a) 1. x_G , 2. y_G; (b) θ_7.

7. Discussion and conclusions

In this paper, trajectory tracking control of parallel manipulators involving flexible-joint drives is analyzed in the presence of modeling error and disturbances. Using the fourth-order input (actuator torques)/output (end-

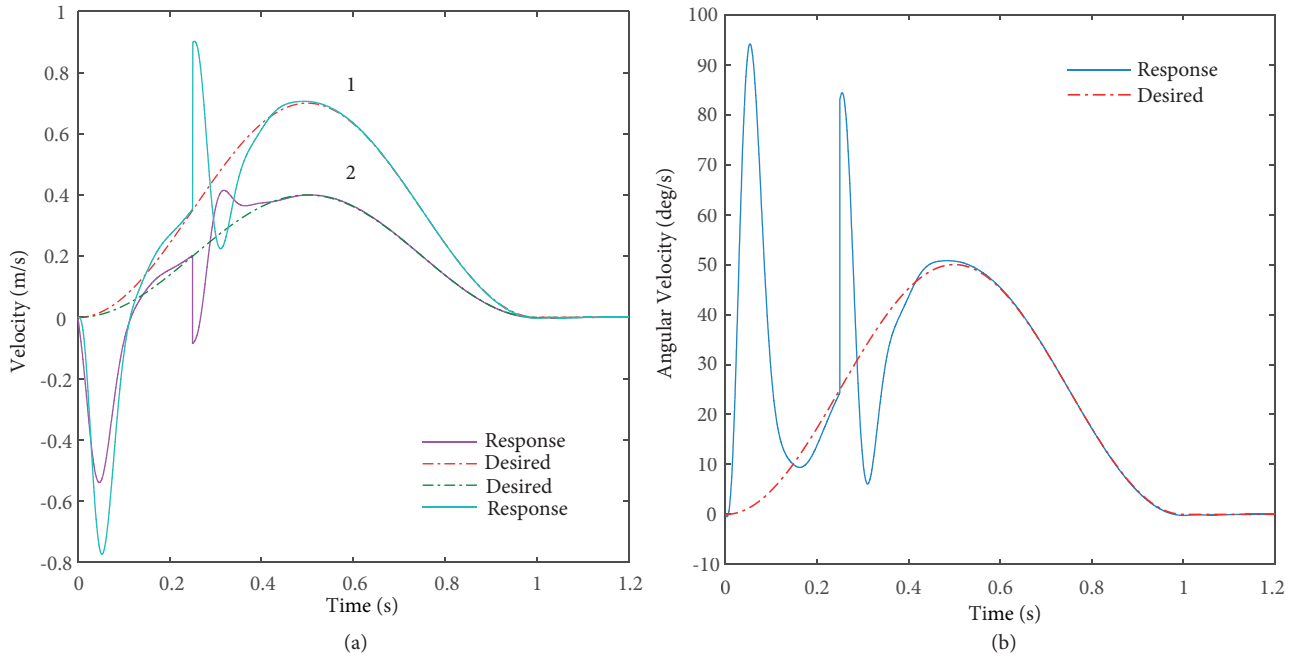

Figure 3. Velocity responses: (a) $1.\dot{x}_G$, $2.\dot{y}_G$; (b) $\dot{\theta}_7$.

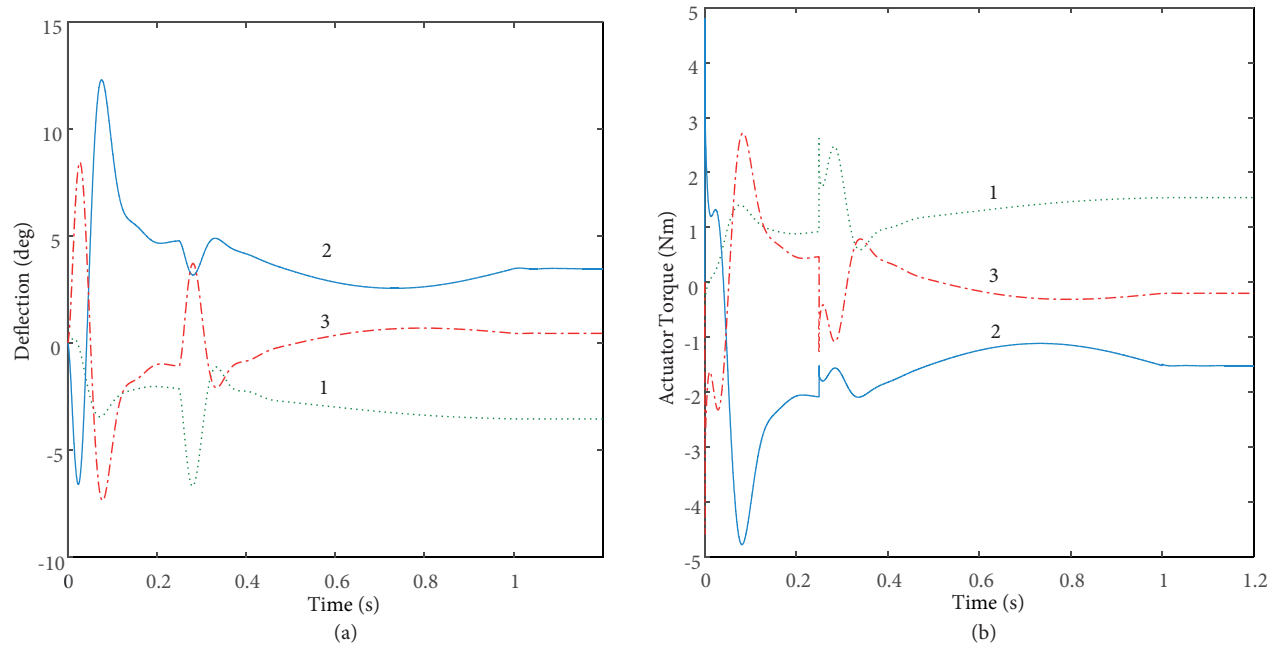

Figure 4. Deflections and actuator torques: (a) $1.\theta_1-\phi_1$, $2.\theta_2-\phi_2$, $3.\theta_3-\phi_3$; (b) $1.T_1^*$, $2.T_2^*$, $3.T_3^*$.

effector displacements) relation obtained by eliminating the intermediate variables, an inverse dynamics control law is utilized. A fourth-order nonhomogeneous linear time-varying error dynamics is obtained. It is shown that by proper selection of the feedback gains the relative variations of the system parameters become sufficiently slow so that the control system becomes stable. Hence, the inverse dynamics control law can be made robust

to parameter uncertainties and disturbances.

A 3-RPR planar parallel manipulator subject to impact is considered as a case study to illustrate the performance of the control method in the presence of 10% modeling error. The impact model involves the impulse momentum equations derived from the dynamic equations and the equation that involves the coefficient of restitution of impact. As expected, the sudden changes in joint velocities due to impact create jumps in the end-effector velocity variables, as well. Indeed, these jumps in the joint velocities represent instantaneous velocity errors that should be compensated by the controller. This, in turn, creates bumps in the position responses and discontinuities in the control torques.

Due to the inertia coupling between the rotor and joint variables, impact affects, in fact, not only the manipulator velocities but also the rotor velocities. However, in the flexible-joint model, the gear ratio is taken sufficiently large, which causes this coupling to be negligible.

Consequently, despite the modeling error, the jump discontinuities that occur because of the impact are suppressed by the control method and a satisfactory tracking performance is achieved. The tracking errors, on the other hand, can be further reduced by increasing the control gains at the expense of increased control torques.

Motor dynamics is neglected in this study in order to focus on the flexible-joint manipulator dynamics since brushless DC motors can be used without considerable lag in the application of the control torques.

As a future work, the effects of friction nonlinearity, link flexibility, backlash at the joints, and saturation limits of the motors on the stability and performance of the inverse dynamics control can be investigated.

References

[1] Good MC, Sweet LM, Strobel KL. Dynamic models for control system design of integrated robot and drive systems. J Dyn Sys Meas Cont 1985, 107: 53-59.

[2] Liu Y, Sun L, Meng Q. Acceleration feedback control of a harmonic drive parallel robot. In: IEEE International Conference on Robotics, Automation and Mechatronics; 1–3 December 2004; Singapore. New York, NY, USA: IEEE. pp. 390-395.

[3] Zhao T, Zhao Y, Shi L, Dai JS. Stiffness characteristics and kinematics analysis of parallel 3-DOF mechanism with flexible joints. In: IEEE International Conference on Mechatronics and Automation; 5–6 August 2007; Harbin, China. New York, NY, USA: IEEE. pp. 1822-1827.

[4] Rong W, Luan Y, Qi L, Sun L. Kinematics analysis and flexible hinge analysis of 3-PPSR precision parallel manipulator. In: IEEE International Conference on Mechatronics and Automation; 5–8 August 2012; Chengdu, China. New York, NY, USA: IEEE. pp. 743-748.

[5] Ider SK, Korkmaz O. Trajectory tracking control of parallel robots in the presence of joint drive flexibility. J Sound Vibr 2009, 319: 77-90.

[6] Korkmaz O, Ider SK. Hybrid force and motion control of flexible joint parallel manipulators using inverse dynamics approach. Adv Rob 2014, 28: 1221-1230.

[7] Liu S, Lu Z, Wu L. Impact dynamics and control of a flexible dual-arm space robot capturing an object. App Maths Comp 2007, 185: 1149-1159.

[8] Angeles J, Zhang DG. Impact dynamics of flexible-joint robots. Comp Str 2005, 83: 25-33.

[9] Qian Z, Zhang D. Impact dynamics of multi-link robots with link and joint flexibility. App Mech Mat 2012, 226: 686-692.

[10] Huang P, Wang D, Meng Z, Zhang F, Liu Z. Impact dynamic modeling and adaptive target capturing control for tethered space robots with uncertainties. IEEE/ASME Trans Mech 2016, 21: 2260-2271.

[11] Spong MW. Modeling and control of elastic joint robots. J Dyn Sys Meas Cont 1987; 109: 310-319.

[12] Ider SK. Inverse dynamics of parallel manipulators in the presence of drive singularities. Mech Mach Theo 2005, 40: 33-44.

[13] Desoer CA. Slowly varying systems $\dot{x}= A(t)x$. IEEE T Automat Contr 1968; 13: 742-743.

[14] Rosenbrook HH. The stability of linear time-dependent control systems. J Electr Cont 1963; 15: 73-80.